Dalton Transactions

Thermo- and photo-induced electron transfer in a series of [Fe2Co2] capsules

Journal:	*Dalton Transactions*
Manuscript ID	DT-ART-10-2022-003328.R1
Article Type:	Paper
Date Submitted by the Author:	16-Dec-2022
Complete List of Authors:	Meng, Lingyi; Southern University of Science and Technology, Chemistry Deng, Yi-Fei; Southern University of Science and Technology, Chemistry; Holmes, Stephen; University of Kentucky, Department of Chemistry and Biochemistry Zhang, Yuan-Zhu; Southern University of Science and Technology, Chemistry

ARTICLE

Thermo- and photo-induced electron transfer in a series of $[Fe_2Co_2]$ capsules

Received 00th January 20xx,
Accepted 00th January 20xx

DOI: 10.1039/x0xx00000x

Lingyi Meng,[#a] Yi-Fei Deng,[#a] Stephen M Holmes,*[b] and Yuan-Zhu Zhang*[a]

Recently, a family of $[Fe_2Co_2]$ molecular capsules that display tunable electron transfer coupled spin transition (ETCST) behaviors were reported via a smart approach through the Schiff-base condensation of aldehyde-functionalized 2,2-bipyridines (bpy^{CHO}) and 1,7-heptanediamine ($H_2N(CH_2)_7NH_2$). Here, three more capsule complexes $\{[(Tp^R)Fe(CN)_3]_2[Co(bpy^{C=N(CH_2)_nN=C}bpy)]_2[ClO_4]_2\}\cdot n(solvent)$ (**1**, Tp^R = Tp*, n = 5, sol = 8DMF; **2**,Tp^R = Tp^{Me}, n = 9, sol = 5MeCN; **3**, Tp^R = Tp*, n = 11, sol = 5MeCN), where Tp* = hydridotris(3,5-dimethylpyrazol-1-yl)borate and Tp^{Me} = hydridotris(3-methylpyrazol-1-yl)borate] are reported, demonstrating a successful extension of such an approach with other alkyldiamines in different lengths. Combined X-ray crystallographic, infrared spectroscopic and magnetic studies reveal incomplete electron transfer with either changing temperature or upon light exposure.

Introduction

Switchable molecule-based materials that display magnetic bistability between two (or more) electronic or spin states have received considerable attention recently as potentially attractive components in switching, display, and information storage applications.[1-4] Among these are well-known Prussian Blue analogues (PBAs), specifically those comprised of cyanide-bridged Fe and Co ions, where reversible electron transfer-coupled spin transition (ETCST) between the $[Fe^{II}_{LS}\text{-}CN\text{-}Co^{III}_{LS}]$ and $[Fe^{III}_{LS}\text{-}CN\text{-}Co^{II}_{HS}]$ units (LS = low spin, HS = high spin) occurs. These changes may be effected in response to various external stimuli such as changing temperature, light, pressure, and electric field.[5-25] Using a variety of chelating ligands, to limit the numbers and directionality of bridging cyanides, a series of molecular building blocks may be selectively inserted into the corners of molecular squares.[11-25] In these complexes, the ETCST behaviour appears to be closely correlated with both the intramolecular (ligand field for both the Fe/Co sites) and intermolecular environments (hydrogen-bonds, π···π stackings, etc.), contributing to the energy separation between the $[Fe^{III}_{LS}\text{-}CN\text{-}Co^{II}_{HS}]$ and $[Fe^{II}_{LS}\text{-}CN\text{-}Co^{III}_{LS}]$ units.[12-24]

While the vast majority of cyanide-based clusters employ pre-assembled ligands, a more recent self-assembly approach exploits post-synthetic modifications (PSMs) as a method to perform late-stage modifications to the ligands present. For example, we recently described the preparation of several hexanuclear complexes $[Fe_2Co_2M_2]$ (M^{2+} = Zn^{2+}, Co^{2+}, Cd^{2+}) derived from molecular squares, via covalent attachment of anionic metal(II) thiocyanates to their respective terminal cyanides.[21] With this modification, the ETCST behaviours of the hexanuclear complexes were promoted towards room temperature, demonstrating the grafted metal complex units may serve as effective electron acceptors, thus enhancing the effective barrier separating the Fe/Co redox tautomeric states.

Schiff-base reactions have been widely applied in the construction of coordination supramolecules, metal-organic frameworks (MOFs), and covalent organic frameworks (COFs).[27-29] As a complimentary strategy, we also explored the synthetic utility to modify coordinated ligands residing in assembled clusters. Given that the formation of dynamic imine covalent linkages (C=N) are usually effective and reversible through a hydrolytic process, a number of mechanically interlocked molecular architectures such as metallacycles, cages or knots have been prepared, showing rich physicochemical properties.[27-30] Inspired by these results, we elected to convert aldehyde-decorated chelating ligands derived from 2,2´-bipyradine (bpy^{CHO}) on dicationic $[Fe_2Co_2]$ square complexes, which undergo Schiff-base condensation in the presence of various amines.[22-24] Interestingly, a series of capsule-like square complexes were prepared, in which the cyanide-bridged $[Fe_2Co_2]$ cores were encapsuled within the long 1,7-heptanediamines.[22-23] Remarkably, these compounds exhibited complete and sharp thermo- and photo-induced ETCST behaviours associated with a first-order phase transition between the Fe^{III}/Co^{II} and Fe^{II}/Co^{III} states, suggesting that significant intermolecular interactions are operative;[22] additional studies revealed the evidenced anion-dependent ETCST behaviour.[23]

As an extension of such works, we reasoned that systematic alteration of alkyl diimines-based bipyridines, would also serve

[a]*Department of Chemistry, Southern University of Science and Technology (SUSTech), Shenzhen, 518055, P. R. China. Email: zhangyz@sustech.edu.cn*
[b]*Department of Chemistry and Biochemistry and Centre for Nanoscience, University of Missouri-St. Louis, St. Louis, Missouri 63121, USA. Email: holmesst@umsl.edu*

†Electronic Supplementary Information (ESI) available: selected bond lengths and angles, crystal structures, thermal gravimetric analysis data, powder X-ray diffraction data and magnetic details. For ESI and crystallographic data in CIF or other electronic format see DOI: 10.1039/x0xx00000x.

# Authors contributed equally to this work.

to modify the packing environment of the clusters, potentially providing better control of the intermolecular environments and separation of clusters in the solid state. In the present contribution, we focused on the preparation of three structurally related clusters via variation of their diamine chain lengths and pyrazolylborate ligands present, $\{[(Tp^{R})Fe(CN)_3]_2[Co(bpy^{C=N(CH2)nN=C}bpy)]_2[ClO_4]_2\}\cdot n(solvent)$, (**1**, Tp^{R} = Tp*, n = 5, sol = 8DMF; **2**,Tp^{R} = Tp^{Me}, n = 9, sol = 5MeCN; **3**, Tp^{R} = Tp*, n = 11, sol = 5MeCN, Tp* = hydridotris(3,5-dimethylpyrazol-1-yl)borate and Tp^{Me} = hydridotris(3-methylpyrazol-1-yl)borate). Combined X-ray crystallographic, variable temperature infrared and magnetic studies revealed that each complex exhibits incomplete thermo- and photo- induced electron transfer, but all display varying degrees of between the paramagnetic $[Fe^{III}_{LS}2Co^{II}_{HS}2]$ and the diamagnetic $[Fe^{II}_{LS}2Co^{III}_{LS}2]$ states.

Results and discussion

Treatment of methanolic solutions of bpy^{CHO} with a series of alkyl diamines $[H_2N(CH_2)_nNH_2$, n = 5/9/11], followed by sequential addition of cobalt(II) perchlorate hexahydrate and $[(Tp^{R})Fe^{III}(CN)_3]^-$ anions, rapidly affords red precipitates. Extraction of the solids into either acetonitrile or DMF, followed by crystallization from layered diethyl ether mixtures, yields a series of imine-functionalized squares of $\{[(Tp^{R})Fe(CN)_3]_2[Co(bpy^{C=N(CH2)nN=C}bpy)]_2[ClO_4]_2\}\cdot n(solvent)$ stoichiometry in modest yields, including the title three complexes.[22,23]

Variable-temperature infrared spectra

Infrared measurements initiated in an effort to determine whether compounds **1**-**3** undergo intramolecular electron transfer (Fig. 1). At 273 K, **1** displays intense and high energy absorptions at 2533, 2154 and 2136 cm^{-1}, which are ascribed to borohydride (ν_{BH}) and bridging and terminal cyanide (ν_{CN}) stretches absorptions belonging to the $[(Tp^*)Fe^{III}(CN)_3]^-$anions present within the $\{Fe^{III}_{LS}(CN)Co^{II}_{HS}\}$ units.[12-23] As the temperature was lowered to 123 K, the ν_{BH} stretch shifts to 2529 cm^{-1} and the intensity of the ν_{CN} bands decrease, while lower energy ones appear [2104, 2083 and 2060 cm^{-1}] being consistent with those belonging to $[Fe^{II}_{LS}(\mu\text{-}CN)Co^{III}_{LS}]$ units.[12-23] For **2** and **3** the high energy ν_{CN} absorptions also seen at 260 K [2158 and 2132 cm^{-1}, **2**; 2154 and 2127 cm^{-1}, **3**] with lower energy ones appearing at lower temperatures [ν_{CN} = 2108 and 2085 cm^{-1} for **2**; 2095, 2072 and 2062 cm^{-1} for **3**]; we note that the intensity of the high energy ν_{CN} changes but never disappears, suggesting that incomplete ETCST occurs in **1**-**3**.

Complexes **2** and **3** appear to be polycrystalline as judged from their powder X-ray diffraction (PXRD) data collected at room temperature. The PXRD data suggests that polycrystalline samples are reasonably robust and resemble those obtained from simulations of their single-crystal X-ray data (Figs. S1–S2). We were unable to obtain analogous PXRD data for **1** indicating that it is predominantly amorphous for facile desolvation results in a rapid loss crystallinity when taken from its mother liquor under experimental conditions. Consistent with this assumption, thermogravimetric analysis (TGA) shows significant mass loss occurs at temperatures below ca. 100 °C (**1**, ca. 21.6%, 8 DMF; **2**, ca. 9.0%, 5 MeCN; **3**, ca. 8.6 %, 5 MeCN) which is consistent with facile removal of lattice solvent in **1** – **3**, respectively (Figs. S3–S5).

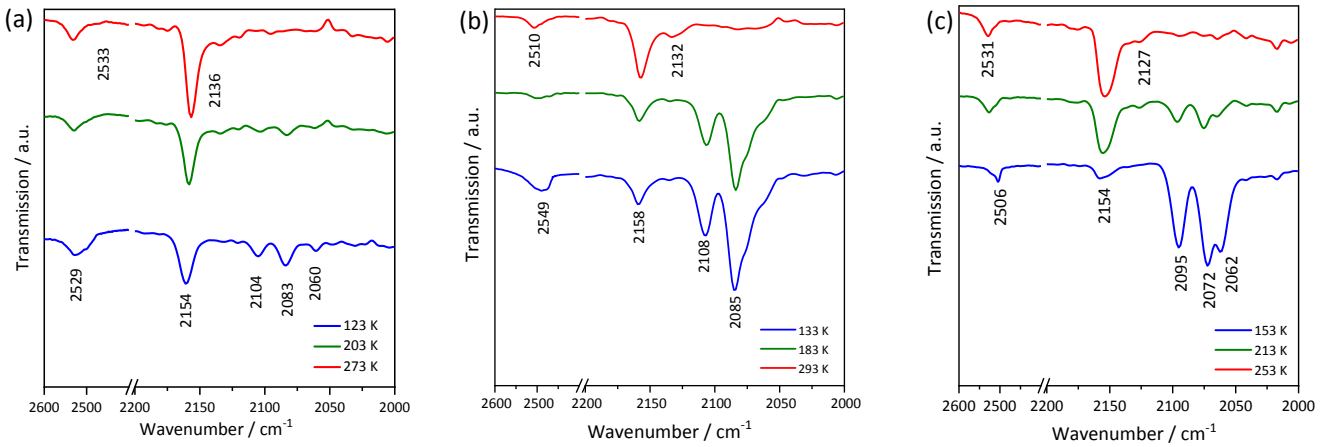

Fig. 1 Variable temperature infrared spectra collected for **1** (a), **2** (b) and **3** (c).

X-ray structural determinations

Single crystal X-ray diffraction data were collected at 100 and 260 K for **1** – **3**, respectively (Table 1). Selected bond lengths and angles are summarized in Tables 2 and S1–S3. Compounds **1** - **3** crystallize in the monoclinic $P2_1/n$, $C2/c$, and triclinic $P\bar{1}$ space groups, respectively, where the asymmetric unit is comprised of half of the molecule square, $[(Tp^{R})Fe(CN)(CN)_2Co(bpy^{imine})]^+$, in addition to lattice solvent(s) and charge-balancing perchlorate anions. The cyanide-bridged and six-coordinate $[(Tp^{R})Fe(CN)_3]^-$ and $[Co(bpy^{imine})_2]^{2+}$ ions reside at alternate corners of the $[Fe_2(\mu\text{-}CN)_4Co_2]^{2+}$ square, leaving a terminal cyanide that adopts an anti-orientation relative to the mean plane of the cluster. The bidentate bpy^{imine} ligands span the face diagonal above and below the mean plane of squares, where each bipyridine coordinates a single cobalt centre, forming a two-handled molecular basket (Fig. 2).

At 260 K, analysis of the crystallographic data shows that the average Co-N bond lengths are rather long [ca. 2.12(4), 2.12(5),

and 2.13(3) Å] for **1** – **3**, respectively, which are comparable to those expected for high spin Co^{II}_{HS} centres (Table 2).[12-23] Below ca. 100 K, the average Co-N distances become slightly shorter [ca. 2.01(6), 2.02(6) and 2.07(5) Å], suggesting that partial or incomplete electron transfer has occurred, being longer than the typical value (ca. 1.9 Å) seen for bona fide Co^{III}_{LS} complexes. As judged from the structural analysis, we propose that **1**-**3** contain significant fractions of both $Fe^{III}_{LS}/Co^{II}_{HS}$ and $Fe^{II}_{LS}/Co^{III}_{LS}$ pairs at 100 K.[13,16] The crystallographic data shows that the average Fe–C≡N bond angles remain nearly linear and invariant with respect to changing crystal temperature, while the Co–N≡C ones become more acute [179.0(5) → 173.0(4)° for **1**; 173.5(5) → 170.6(5)° for **2**, and 168.7(4) → 164.7(4)° for **3**], between 260 to 100 K, respectively. We also find that the Fe-C≡N-Co linkages become more distorted as a function of increasing alkyl chain length (e.g., **1** < **2** < **3**) when structures at 100 K are compared to those at 260 K, confirming that Fe^{II}/Co^{III} pairs have been thermally converted to Fe^{III}/Co^{II} ones, suggesting that the Co^{III}_{LS} to Co^{II}_{HS} conversion induces significant lattice strain between adjacent $[Fe_2Co_2]$ clusters within the lattice.

The solid state packing environment at 260 K reveals considerable intermolecular edge-to-edge π···π interactions between adjacent bipyridine (bpy) ligands [**1**, 3.549 Å; **2**, 3.964 Å; **3**, 3.773 Å] and between bpy and Tp^{Me} ligands (**1**, 3.727 Å), and those of C-H···π interactions between the alkyl chain and bpy or Tp* ligands (**2**, 3.676, 3.772 Å; **3**, 3.823 Å). The nearest intermolecular metal-metal distances are ca. 10.36, 12.76 and 11.55 Å for **1** – **3** at 260 K, respectively confirming the separation of the $[Fe_2(CN)_4Co_2]^{2+}$ cores (Figs. S9–S11).

Table 1 Crystal data and structure refinement for **1** – **3**.

Complex	**1**		**2**		**3**	
temperature, K	100(2)	260(2)	100(2)	260(2)	100(2)	260(2)
formula	$C_{118}H_{160}B_2Cl_2Co_2Fe_2N_{38}O_{16}$		$C_{106}H_{121}B_2Cl_2Co_2Fe_2N_{35}O_8$		$C_{116}H_{143}B_2Cl_2Co_2Fe_2N_{35}O_8$	
molecular weight (g mol^{-1})	2688.42		2335.29		2477.73	
crystal system	monoclinic		monoclinic		triclinic	
space group	$P2_1/n$		$C2/c$		$P\bar{1}$	
a, Å	21.745(3)	22.146(3)	22.863(1)	23.019(4)	14.0286(7)	14.246(2)
b, Å	14.665(2)	14.840(2)	17.548(1)	17.917(3)	15.5718(8)	15.814(2)
c, Å	21.799(2)	22.231(3)	27.236(2)	27.567(5)	16.0029(8)	16.329(2)
α, deg	90	90	90	90	73.466(2)	72.318(5)
β, deg	109.157(4)	109.343(4)	91.011(2)	91.420(7)	74.402(2)	73.993(5)
γ, deg	90	90	90	90	70.073(2)	69.773(5)
V, Å^3	6566(1)	6894(1)	10925(1)	11366(4)	3093(3)	3228(8)
Z	2	2	4	4	1	1
ρ_{cal}, g cm^{-3}	1.138	1.084	1.345	1.296	1.330	1.258
2ϑ range, °	4.71 - 49.61	4.63 - 49.61	4.61 - 49.62	4.55 - 49.56	4.52 - 52.98	4.46 - 53.16
Completeness	99%	100%	100%	99%	100%	100%
Residual map, *e* Å^{-3}	0.79/-1.08	0.65/-0.55	0.82/-1.55	0.89/-0.90	1.90/-0.87	0.97/-0.53
Goodness-of-fit on F^2	1.012	1.022	1.102	1.117	1.040	1.032
Final indices [$I > 2\sigma(I)$]	R_1 = 0.0869, wR_2 = 0.2238	R_1 = 0.0693, wR_2 = 0.1843	R_1 = 0.0904, wR_2 = 0.2364	R_1 = 0.0745, wR_2 = 0.1962	R_1 = 0.0820, wR_2 = 0.2146	R_1 = 0.0560, wR_2 = 0.1630
R indices (all data)	R_1 = 0.1274, wR_2 = 0.2609	R_1 = 0.0993, wR_2 = 0.2114	R_1 = 0.1139, wR_2 = 0.2573	R_1 = 0.0973, wR_2 = 0.2140	R_1 = 0.1093, wR_2 = 0.2349	R_1 = 0.0815, wR_2 = 0.1869

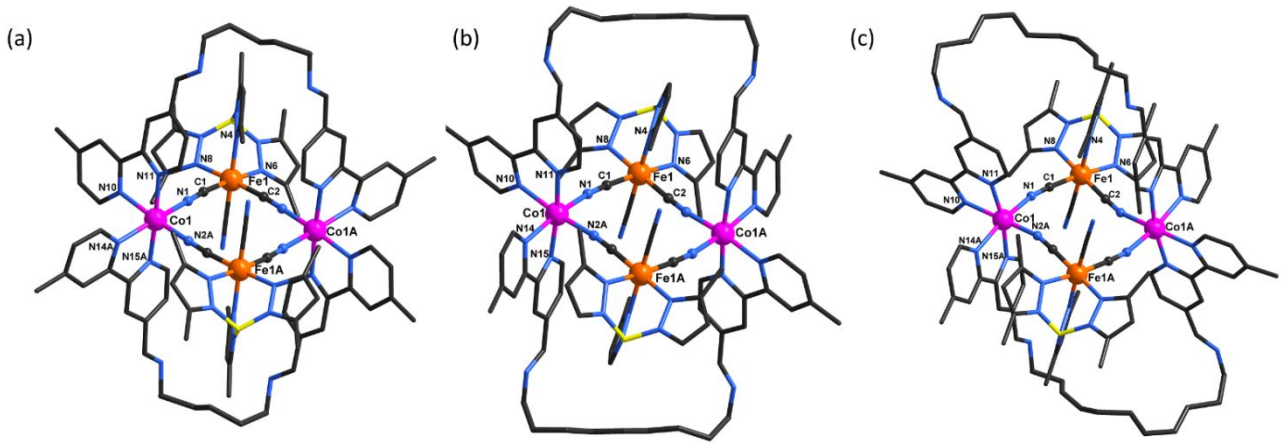

Fig. 2 Wire representation of the X-ray structures of **1** (a), **2** (b) and **3** (c) at 260 K. All lattice solvents, hydrogen atoms, and anions are eliminated for clarity.

ARTICLE

Table 2 Selected bond lengths [Å] and angles (°) for **1** – **3**.

Complex	1		2		3	
	100 K	260 K	100 K	260 K	100 K	260 K
Co1-N1 [Å]	1.986(5)	2.073(4)	1.995(6)	2.076(4)	2.019(4)	2.077(3)
Co1-N11 [Å]	2.028(5)	2.133(3)	2.029(6)	2.119(5)	2.077(4)	2.128(3)
Co1-N10 [Å]	2.016(6)	2.126(4)	2.038(6)	2.128(4)	2.100(4)	2.146(3)
Co1-N2A [Å]	1.968(5)	2.103(4)	1.988(5)	2.080(4)	2.058(4)	2.134(3)
Co1-N14(A) [Å]	2.019(5)	2.121(3)	2.050(6)	2.145(4)	2.096(5)	2.157(3)
Co1-N15(A) [Å]	2.040(5)	2.153(3)	2.048(5)	2.136(4)	2.084(5)	2.131(3)
Co-$N_{ave.}$ [Å]	2.01(6)	2.12(4)	2.02(6)	2.11(5)	2.07(5)	2.13(3)
Fe1-C1-N1 [˚]	174.6(4)	175.8(4)	175.3(5)	176.7(4)	174.8(4)	176.2(3)
Fe1-C2-N2 [˚]	174.7(5)	175.1(4)	177.8(6)	177.3(5)	179.0(4)	177.4(3)
Co1-N1-C1 [˚]	173.0(4)	179.4(4)	173.5(5)	173.2(4)	168.7(4)	168.7(3)
Co1A-N2-C2 [˚]	179.0(5)	173.3(3)	170.6(5)	172.4(4)	164.7(4)	166.0(3)
Σ_{Co}[a] [˚]	62.02(2)	75.04(1)	57.40(1)	67.29(2)	60.86(2)	66.91(1)
$CShM_{Co}$[b]	0.763	1.267	0.714	1.076	0.721	0.933

[a] Σ_{Co} : the sum of $|90-\alpha|$ for the 12 *cis*-N-Co-N angles around the cobalt atom; [b] $CShM_{Co}$: the continuous shape measurement relative to ideal octahedron of the Co centre.

Magnetic studies

The magnetic susceptibility data for **1** – **3** were collected between 2-300 K under an applied static magnetic field (H_{dc} = 1 kOe) (Fig. 3). At 300 K, the χT product for **1**-**3** are comparable [6.59, 6.66, and 6.62 cm^3 K mol^{-1}] and are in the range expected for paramagnetic [$Fe^{III}_2Co^{II}_2$] complexes containing a 2:2 ratio of low spin Fe(III) (S = ½, g = 2.5 ~ 2.7) and high spin Co(II) (S = $^3/_2$, g = 2.0 ~ 2.8) ions.[12,31] As the temperature is lowered, the χT values for **1**-**3** remain nearly constant until ca. 230 K, and then gradually approach smaller ones [3.38, 3.02, and 3.56 cm^3 K mol^1], possibly indicating that approximately half of the paramagnetic Fe/Co pairs have been converted to diamagnetic ones. We were initially excited to see possible evidence of an intermediate state, [$Fe^{III}Co^{II}Fe^{II}Co^{III}$], or a phase containing a 1:1 mixture of paramagnetic [$Fe^{III}_2Co^{II}_2$] and diamagnetic [$Fe^{II}_2Co^{III}_2$] complexes. Unfortunately, we were unable to obtain crystallographic evidence to support this hypothesis, that is, no supercell or localized changes in the Co-N distances are seen structures of **1**-**3**. As judged from the magnetic data, thermal transition temperatures ($T_{1/2}$), the point where half of the clusters simultaneously exist in the Fe^{II}/Co^{III} and Fe^{III}/Co^{II} states, are estimated to occur at ca. 170, 188, and 165 K for **1** - **3**, respectively. The absence of significant thermal hysteresis in the magnetic data suggests that the transformation of Fe^{II}/Co^{III} into Fe^{III}/Co^{II} pairs occurs without intermolecular cooperativity. We hypothesize that this may be reflective of well-separated clusters in the solid state, leading to inefficient elastic interactions, strain propagation, and volume expansion associated with Co^{III}_{LS}-N to Co^{II}_{HS}-N bonds upon reduction.[32-33] When the temperature is again brought to room temperature, the χT products are seen to return to their original values, suggesting that thermally-induced changes in their magnetization are indeed reversible.

The behaviours of **1**- **3** were also investigated at 10 K under the presence of light irradiation [Figs. 3 and S12–S14]. Upon irradiation [808 nm] for 1 h, the χT products of **1** – **3** quickly approach their expected saturation values [7.89, 6.92 and 7.07 cm^3 K mol^{-1}] indicating that facile photo transformation of Fe^{II}/Co^{III} into metastable paramagnetic [$Fe^{III}_{LS2}Co^{II}_{HS2}$] ones is possible at cryogenic temperatures [Figs. S12–S14]. Upon removal of the light source, samples were heated from 2 to 12 K, whereby the χT values increased from 4.21 to 7.89 cm^3 K mol^{-1} for **1**, 2.89 to 6.92 cm^3 K mol^{-1} for **2**, and 3.47 to 7.07 cm^3 K mol^{-1} for **3**, which is ascribed to the intermolecular antiferromagnetic interactions between the photogenerated paramagnetic Fe^{III}/Co^{II} pairs as well as the magnetic anisotropy (zero-field splitting) of metal centres.[12-25] At higher temperatures, there is sufficient thermal energy to overcome the magnetic exchange interactions (ca. 3-6 cm^{-1}) and the Fe^{III} and Co^{II} ions adopt a metastable paramagnetic state. To gain an insight into this metastable state, the photo-irradiated magnetic susceptibility data at 2 – 50 K for **1** - **3** were fitted using PHI program[34] (Fig. S15) based on the following spin Hamiltonian (eq. 1):

$$\hat{H} = -2J(\hat{S}_{Fe1}\hat{S}_{Co1} + \hat{S}_{Fe1}\hat{S}_{Co1A} + \hat{S}_{Fe1A}\hat{S}_{Co1} + \hat{S}_{Fe1A}\hat{S}_{Co1A}) + \sum_i (D_{Co,i}\hat{S}^2_{z,i} + g_{Co,i}\mu_B B\hat{S}_{Co,i} + g_{Fe,i}\mu_B B\hat{S}_{Fe,i})$$

Where D, μ_B, g, B and J correspond to the axial zero-field splitting (zfs) parameter, Bohr magneton, Landé factor, magnetic field vector, and magnetic exchange between Co(II) and Fe(III) metal centres, respectively. To avoid the overparameterization, g_{Fe} is fixed as 2.6 based on the previous related literature.[35] Given that the significant π-π stackings, a *zj'* corresponds to the intermolecular interactions has also been included, the best fitting gave:

Table 3 Experimental (PHI) fitting results for complexes **1** - **3**.

Compd.	**1**	**2**	**3**
D (cm^{-1})	40.8	30.2	29.4
J (cm^{-1})	4.6	3.4	5.8
zj' (cm^{-1})	-0.1	-0.2	-0.1
g_{Co}	2.6	2.7	2.3
g_{Fe} (fixed)	2.6	2.6	2.6

The zfs fitting parameters for **1** – **3** are comparable to those reported high-spin Co(II) in a distorted octahedral coordination environment.[36] The obtained *J* and *zj'* parameters suggest the intra-ferromagnetic and inter-antiferromagnetic interactions, respectively. These results corroborate both the intermolecular antiferromagnetic interactions and magnetic anisotropy would contribute to the low temperature decrease of χT products. With additional heating, the magnetically isolated Fe^{III} and Co^{II} ions state returns to the thermodynamically preferred diamagnetic Fe^{II}/Co^{II} one, at temperatures above ca. 112, 132 and 132 K, for **1**-**3**, respectively.

In prior studies we demonstrated that rather sharp and nearly complete intramolecular electron transfer occurs in $[Fe_2Co_2]$ capsules (**R1**), derived from pentylbis(imino-pyridine) ligands. Curiously, the cationic portions of **1** and **R1**, are identical, in that they each contain the same ancillary ligands. However, their solid-state intermolecular environments and charge-balancing anions present are different [ClO_4^- vs PF_6^-], as well as the temperature regimes where intramolecular electron transfer is operative. Furthermore, thermal hysteresis is observed in one (**R1**) but not the latter (**1**), suggesting that intermolecular contacts may be important. Most notable is the observation that **1** displays negligible thermal hysteresis (ca. 2 K) while **R1** has a pronounced one (ca. 6 K), suggesting that intermolecular contacts may be more important role in their disparate behaviours.

In the frame of Marcus-Hush electron transfer, the magnetic transition is likely to be strongly correlated with the local coordination environment (ligand field, ΔG) and possibly intermolecular ligand-ligand interactions (reorganization energy, λ). These factors are highlighted in derivatives containing various anions and lattice solvents (**1**, ClO_4, 8DMF; **R1**, PF_6, 6DMF) and those derived from other bipyridine and pyrazolylborate ligands.[12-18, 21-24] These factors are expected to play subtle but important roles in modulating intermolecular environments, ligand fields, and ultimately the temperature regimes whereby thermo- and photochromic behaviour may be observed. As shown in Tables 2 and S4, the continuous shape analysis shows that at 260 K, both the distortion parameters Σ and $CShM_{Co}$ for **1** (75.04° and 1.267) are larger than those of **R1** (72.50° and 1.157), suggesting a weaker cobalt ligand field, which would potentially lower the energy separation between the Fe^{III}/Co^{II} and Fe^{II}/Co^{III} states. If this assumption is correct, a lower thermal transition temperature ($T_{1/2}$) is expected. It follows that less distorted and more separated structures (like **R1**) may engender higher ligand field and reorganization energies which ultimately lead to correspondingly higher thermal phase transition temperatures (e.g., **1**, 170 K vs **R1**, 230 K).

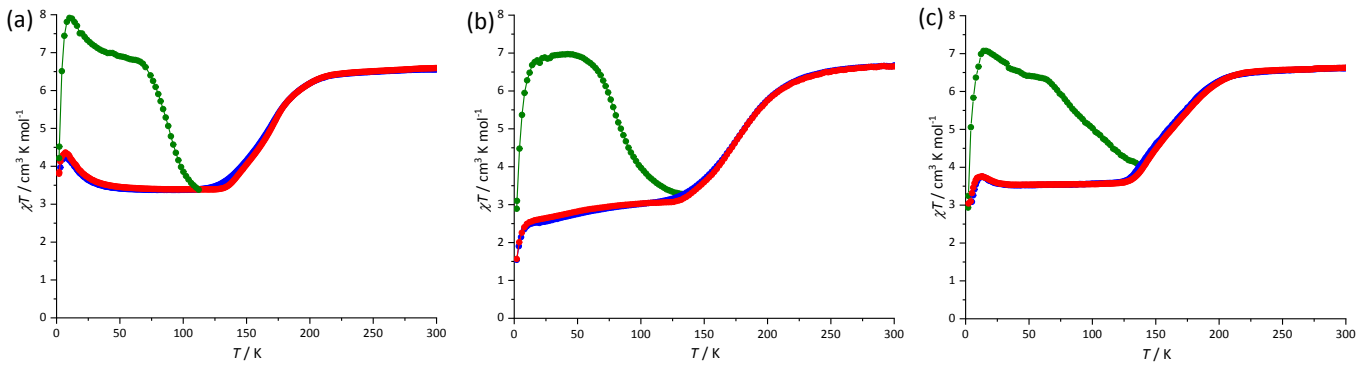

Fig. 3 Variable temperature magnetic susceptibility data for **1** (a), **2** (b) and **3** (c) collected in the dark (1 kOe; blue, cooling; red, heating) and after light irradiation (808nm, 20 mW, green, 10 kOe) at 10 K. Solid lines are guides for the eye.

Conclusions

In summary, we have described the synthesis, structural, spectroscopic, and magnetic properties of three cyanide-bridged molecular squares. We find that judicious substitution of ancillary ligands within a common tetranuclear structural archetype offers an attractive strategy to systematically alter changes in their observed thermo- and photochromic behaviour. We propose that these changes may be related to intermolecular interactions that change both their resulting ligand field (at Co) and elastic interactions associated with electron transfer, spin state, and volume changes in the solid

state. Analysis of several complimentary data suggests that incomplete intramolecular electron transfer may be associated with the existence of an intermediate spin and tautomeric states. Future efforts are directed towards a better understanding of these attributes with an ultimate goal of preparing multifunctional materials.

Conflicts of interest

There are no conflicts to declare.

Acknowledgements

This work was supported by the National Science Foundation (CHE-1214063 and CHE-1800578, S.M.H.), the Stable Support Plan Program of Shenzhen Natural Science Fund (No. 20200925151834005, Y.Z.Z.), Guangdong Basic and Applied Basic Research Foundation (No. 2022A1515011818, Y.F.D.), and the National Natural Science Foundation of China (No. 21901108, Y.F.D.; No. 22173043, Y.Z.Z.).

Notes and references

(1) (a) Z.-S. Yao, Z. Tang and J. Tao, *Chem. Commun.*, 2020, **56**, 2071; (b) V. Rubio-Giménez, S. Tatay and C. Martí-Gastaldo, *Chem. Soc. Rev.*, 2020, **49**, 5601-5638; (c) M. Feng, Z.-Y. Ruan, Y.-C. Chen and M.-L. Tong, *Chem. Commun.*, 2020, **56**, 13702-13718; (d) K. S. Kumar and M. Ruben, *Coord. Chem. Rev.*, 2017, **346**, 176–205.

(2) (a) M. Nakaya, R. Ohtani, L. F. Lindoy and S. Hayami, *Inorg. Chem. Front.*, 2021, **8**, 484-498; (b) M. Wang, Z.-Y. Li, R. Ishikawa and M. Yamashita, *Coord. Chem. Rev.*, 2021, **435**, 213819; (c) M. Reczyński, K. Nakabayashi and S. Ohkoshi, *Eur. J. Inorg. Chem.*, 2020, **2020**, 2669−2678.

(3) (a) O. Sato, J. Tao and Y.-Z. Zhang, *Angew. Chem., Int. Ed.*, 2007, **46**, 2152–2187; (b) O. Sato, *Nat. Chem.*, 2016, **8**, 644–656; (c) S. Ohkoshi and H. Tokoro, *Acc. Chem. Res*., 2012, **45**, 1749–1758; (d) S. Chorazy, J. J. Zakrzewski, M. Magott, T. Korzeniak, B. Nowicka, D. Pinkowicz, R. Podgajny and B. Sieklucka, *Chem. Soc. Rev.*, 2020, **49**, 5945-6001.

(4) (a) L. Zhao, Y.-S. Meng, Q. Liu, O. Sato, Q. Shi, H. Oshio and T. Liu, *Nat. Chem.*, 2021, **13**, 698–704; (b) X.-H. Zhao, D. Shao, J.-T. Chen, D.-X. Gan, J. Yang and Y.-Z. Zhang, *Sci. China: Chem.*, 2022, **65**, 532−538; (c) X.-H. Zhao, D. Shao, J.-T. Chen, M. Liu, T. Li, J. Yang and Y.-Z. Zhang, *Dalton Trans*., 2021, **50**, 9768-9774.

(5) (a) D. Aguilà, Y. Prado, E. S. Koumousi, C. Mathonière and R. Clérac, *Chem. Soc. Rev.*, 2016, **45**, 203–224; (b) Y.-S. Meng, O. Sato and T. Liu, *Angew. Chem., Int. Ed.*, 2018, **57**, 12216–12226; (c) Y.-S. Meng and T. Liu, *Acc. Chem. Res*., 2019, **52**, 1369–1379; (d) C. Mathonière, *Eur. J. Inorg. Chem.*, 2018, **2018**, 248−258; (e) G. N. Newton, M. Nihei and H. Oshio, *Eur. J. Inorg. Chem.*, 2011, **2011**, 3031−3042.

(6) Y. Li, A. Benchohra, B. Xu, B. Baptiste, K. Béneut, P. Parisiades, L. Delbes, A. Soyer, K. Boukheddaden and R. Lescouëzec, *Angew. Chem., Int. Ed.*, 2020, **59**, 17272−17276.

(7) (a) M. You, D.-X. Gan, Y.-F. Deng, D. Shao, Y.-S. Meng, X.-Y. Chang and Y.-Z. Zhang, *CCS Chem*., 2021, **3**, 2593-2600; (b) W. Wen, Y.-S. Meng, C.-Q. Jiao, Q. Liu, H.-L. Zhu, Y.-M. Li, H. Oshio and T. Liu, *Angew. Chem., Int. Ed.*, 2020, **59**, 16393−16397; (c) M. Reczyński, D. Pinkowicz, K. Nakabayashi, C. Näther, J. Stanek, M. Kozieł, J. Kalinowska-Tłuścik, B. Sieklucka, S. Ohkoshi and B. Nowicka, *Angew. Chem., Int. Ed.*, 2021, **60**, 2330−2338; (d) J.-R. Jiménez, J. Glatz, A. Benchohra, G. Gontard, L.-M. Chamoreau, J.-F. Meunier, A. Bousseksou and R. Lescouëzec, *Angew. Chem., Int. Ed.*, 2020, **59**, 8089−8093.

(8) O. Sato, T. Iyoda, A. Fujishima and K. Hashimoto, *Science*, 1996, **272**, 704−705.

(9) C. P. Berlinguette, A. Dragulescu-Andrasi, A. Sieber, J. R. Galán-Mascarós, H.-U. Güdel, C. Achim and K. R. Dunbar, *J. Am. Chem. Soc.*, 2004, **126**, 6222−6223.

(10) D. Li, R. Clérac, O. Roubeau, E. Harté, C. Mathonière, R. Le Bris and S. M. Holmes, *J. Am. Chem. Soc.*, 2008, **130**, 252−258.

(11) (a) D. Garnier, J.-R. Jiménez, Y. Li, J. von Bardeleben, Y. Journaux, T. Augenstein, E. M. B. Moos, M. T. Gamer, F. Breher and R. Lescouëzec, *Chem. Sci.*, 2016, **7**, 4825−4831; (b) J.-R. Jiménez, M. Tricoire, D. Garnier, L.-M. Chamoreau, J. von Bardeleben, Y. Journaux, Y. Li and R. Lescouëzec, *Dalton Trans.*, 2017, **46**, 15549-15557.

(12) Y.-Z. Zhang, D. Li, R. Clérac, M. Kalisz, C. Mathonière and S. M. Holmes, *Angew. Chem., Int. Ed.*, 2010, **49**, 3752−3756.

(13) M. Nihei, Y. Sekine, N. Suganami, K. Nakazawa, A. Nakao, H. Nakao, Y. Murakami and H. Oshio, *J. Am. Chem. Soc.*, 2011, **133**, 3592−3600.

(14) Y.-Z. Zhang, P. Ferko, D. Siretanu, R. Ababei, N. P. Rath, M. J. Shaw, R. Clérac, C. Mathonière and S. M. Holmes, *J. Am. Chem. Soc.*, 2014, **136**, 16854−16864.

(15) (a) L. Cao, J. Tao, Q. Gao, T. Liu, Z. Xia and D. Li, *Chem. Commun*., 2014, **50**, 1665−1667; (b) C. Zheng, J. Xu, Z. Yang, J. Tao and D. Li, *Inorg. Chem.*, 2015, **54**, 9687−9689.

(16) (a) Y. Sekine, M. Nihei and H. Oshio, *Chem. - Eur. J.*, 2017, **23**, 5193−5197; (b) M. Nihei, Y. Yanai, I.-J. Hsu, Y. Sekine and H. Oshio, *Angew. Chem., Int. Ed.*, 2017, **56**, 591−594; (c) M. Nihei, Y. Yanai, D. Natke, R. Takayama, M. Kato, Y. Sekine, F. Renz and H. Oshio, *Chem. - Eur. J.*, 2019, **25**, 7449−7452; (d) M. Nihei, K. Shiroyanagi, M. Kato, R. Takayama, H. Murakami, Y. Kera, Y. Sekine and H. Oshio, *Inorg. Chem.*, 2019, **58**, 11912−11919.

(17) D. Siretanu, D. Li, L. Buisson, D. M. Bassani, S. M. Holmes, C. Mathonière and R. Clérac, *Chem. - Eur. J.*, 2011, **17**, 11704−11708.

(18) (a) C.-Q. Jiao, W.-J. Jiang, Y.-S. Meng, W. Wen, L. Zhao, J.-L. Wang, J.-X. Hu, G. G. Gurzadyan, C.-Y. Duan and T. Liu, *Nat. Sci. Rev.*, 2018, **5**, 507−515; (b) C.-Q. Jiao, Y.-S. Meng, Y. Yu, W.-J. Jiang, W. Wen, H. Oshio, L. Luo, C.-Y. Duan and T. Liu, *Angew. Chem., Int. Ed.*, 2019, **58**, 17009−17015.

(19) (a) J. Mercurol, Y. Li, E. Pardo, O. Risset, M. Seuleiman, H. Rousselière, R. Lescouëzec and M. Julve, *Chem. Commun.*, 2010, **46**, 8995−8997; (b) A. Mondal, Y. Li, M. Seuleiman, M. Julve, L. Toupet, M. Buron-Le Cointe and R. Lescouëzec, *J. Am. Chem. Soc.*, 2013, **135**, 1653−1656; (c) S. De, J.-R. Jiménez, Y. Li, L.-M. Chamoreau, A. Flambard, Y. Journaux, A. Bousseksou and R. Lescouëzec, *RSC Adv.*, 2016, **6**, 17456−17459; (d) S. Kamilya, S. Ghosh, Y. Li, P. Dechambenoit, M. Rouzières, R. Lescouëzec, S. Mehta and A. Mondal, *Inorg. Chem.*, 2020, **59**, 11879−11888.

(20) J. Yadav, D. J. Mondal and S. Konar, *Chem. Commun.*, 2021, **57**, 5925−5928.

(21) S. Liu, Y.-F. Deng, Z.-Y. Chen, L. Meng, X. Chang, Z. Zheng and Y.-Z. Zhang, *CCS Chem*., 2020, **2**, 2530-2538.

(22) L. Meng, Y.-F. Deng, S. Liu, Z. Zheng and Y.-Z. Zhang, *Sci. China: Chem.*, 2021, **64**, 1340−1348.

(23) L. Meng, Y.-F. Deng and Y.-Z. Zhang, *Inorg. Chem.*, 2021, **60**, 14330−14335.

(24) L. Meng, Y.-F. Deng, J. Liu, Y. J. Liu and Y.-Z. Zhang, *Dalton Trans.*, 2022, **51**, 15669−15674.

(25) (a) E. S. Koumousi, I.-R. Jeon, Q. Gao, P. Dechambenoit, D. N. Woodruff, P. Merzeau, L. Buisson, X. Jia, D. Li, F. Volatron, C. Mathonière and R. Clérac, *J. Am. Chem. Soc.*, 2014, **136**, 15461−15464; (b) S. F. Jafri, E. S. Koumousi, M.-A. Arrio, A. Juhin, D. Mitcov, M. Rouzieres, P. Dechambenoit, D. Li, E. Otero, F. Wilhelm, A. Rogalev, L. Joly, J.-P. Kappler, C. Cartier dit Moulin, C. Mathonière, R. Clérac and P. Sainctavit, *J. Am. Chem.Soc.,* 2019, **141**, 3470−3479.

(26) (a) T. Liu, Y.-J. Zhang, S. Kanegawa and O. Sato, *J. Am. Chem. Soc.*, 2010, **132**, 8250−8251; (b) D.-P. Dong, T. Liu, S. Kanegawa, S. Kang, O. Sato, C. He and C.-Y. Duan, *Angew. Chem., Int. Ed.,* 2012, **51**, 5119−5123; (c) N. Hoshino, F. Iijima, G. N. Newton, N. Yoshida, T. Shiga, H. Nojiri, A. Nakao, R. Kumai, Y. Murakami and H. Oshio, *Nat. Chem.*, 2012, **4**, 921−926; (d) J.-X. Hu, L. Luo, X.-J. Lv, L. Liu, Q. Liu, Y.-K. Yang, C.-Y. Duan, Y. Luo and T. Liu, *Angew. Chem., Int. Ed.,* 2017, **56**, 7663−7668; (e) J. Li, S. Wu, S. Su, S. Kanegawa and O. Sato, *Chem. - Eur. J.*, 2020, **26**, 3259−3263.

(27) (a) M. Hardy, J. Tessarolo, J. J. Holstein, N. Struch, N. Wagner, R. Weisbarth, M. Engeser, J. Beck, S. Horiuchi, G. H. Clever and A. Lützen, *Angew. Chem., Int. Ed.,* 2021, **60**, 22562 − 22569; (b) D. Zhang, T. K.

Ronson and J. R. Nitschke, *Acc. Chem. Rev.*, 2018, **51**, 2423-2436; (c) A. M. Castilla, W. J. Ramsay and J. R. Nitschke, *Acc. Chem. Rev.*, 2014, **47**, 2063-2073.
(28) (a) C. Sarkar, S. C. Shit, N. Das and J. Mondal, *Chem. Commun.,* 2021, **57**, 8550-8567; (b) P. J. Waller, F. Gándara and O. M. Yaghi, *Acc. Chem. Rev.*, 2015, **48**, 3053-3063.
(29) (a) M. Kaur, S. Kumar, M. Yusuf, J. Lee, R. J. C. Brown, K.-H. Kim and A. K. Malik, *Coord. Chem. Rev.*, 2021, **449**, 214214; (b) S. M. Cohen, *Chem. Rev.*, 2012, **112**, 970-1000.
(30) T. K. Ronson, J. P. Carpenter and J. R. Nitschke, *Chem*, 2022, **8**, 557-568.
(31) F. Lloret, M. Julve, J. Cano, R. Ruiz-García and E. Pardo, *Inorg. Chim. Acta*, 2008, **361**, 3432-3445.
(32) M. Cammarata, S. Zerdane, L. Balducci, G. Azzolina, S. Mazerat, C. Exertier, M. Trabuco, M. Levantino, R. Alonso-Mori, J. M. Glownia, S. Song, L. Catala, T. Mallah, S. F. Matar and E. Collet, *Nat. Chem.*, 2021, **13**, 10-14.
(33) S. Zerdane, M. Hervé, S. Mazerat, L. Catala, R. Alonso-Mori, J. M. Glownia, S. Song, M. Levantino, T. Mallah, M. Cammarata and E. Collet, *Faraday Discuss.*, 2022, **237**, 224-236.
(34) N. F. Chilton, R. P. Anderson, L. D. Turner, A. Soncini and K. S. Murray, *J. Comput. Chem.*, 2013, **34**, 1164−1175.
(35) J. Yang, X.-H. Zhao, Y.-F. Deng, X.-Y. Zhang, X.-Y. Chang, Z. Zheng and Y.-Z. Zhang, *Inorg. Chem.*, 2020, **59**, 16215−16224.
(36) J. M. Frost, K. L. M. Harriman and M. Murugesu, *Chem. Sci.*, 2016, **7**, 2470–2491.